Modelling and Compensating Measurement Errors Caused by Scattering in Time-Of-Flight Cameras

Tom Kavli[a], Trine Kirkhus*[a], Jens T Thielemann[a], Borys Jagielski [b]
[a]SINTEF ICT, Pb. 124 Blindern, N-0314 Oslo, Norway;
[b]University of Oslo, Pb. 1072 Blindern, N-0316, Oslo, Norway

ABSTRACT

Recently, Range Imaging (RIM) cameras have become available that capture high resolution range images at video rate. Such cameras measure the distance from the scene for each pixel independently based upon a measured time of flight (TOF). Some cameras, such as the SwissRanger™ SR-3000, measure the TOF based on the phase shift of reflected light from a modulated light source. Such cameras are shown to be susceptible to severe distortions in the measured range due to light scattering within the lens and camera. Earlier work induced using a simplified Gaussian point spread function and inverse filtering to compensate for such distortions. In this work a method is proposed for how to identify and use generally shaped empirical models for the point spread function to get a more accurate compensation. The otherwise difficult inverse problem is solved by using the forward model iteratively, according to well established procedures from image restoration. Each iteration is done as a sequential process, starting with the brightest parts of the image and then moving sequentially to the least bright parts, with each step subtracting the estimated effects from the measurements. This approach gives a faster and more reliable compensation convergence. An average reduction of the error by more than 60% is demonstrated on real images. The computation load corresponds to one or two convolutions of the measured complex image with a real filter of the same size as the image.

Keywords: Time of flight camera, range imaging, optical scattering, empirical determination of Point Spread Function

1. INTRODUCTION

Systems for measuring 3D geometries of objects or scenes can be used for a variety of applications, such as reverse engineering, scene mapping, robot navigation, and video surveillance. Commonly the technologies are scanner based, measuring each point sequentially (e.g. laser scanners), triangulation methods (e.g. stereo vision and photogrammetry), and interferometric methods. Some drawbacks of these techniques include long measurement times for scanners, challenging image analysis for stereo imaging, and limited depth range for interferometic methods.

Recently Range Imaging (RIM) cameras have become available that capture high resolution range images at video rate without any need for image processing. Such cameras measures the distance to the scene for each pixel independently based upon a measured *time of flight (TOF)*, the time the light needs to travel from a light source near the camera to the target object and back to the camera. The time of flight is measured based on one of two principles:

1. **Pulse travel time.** The camera measures the travel time from a short pulse of light that is emitted until it is received at the detector, using a high resolution timing device [1].
2. **Phase shift of modulated light.** The camera measures the phase shift between the light emitted from a modulated light source and the light received at the detector. The computed distance is proportional to this phase shift [2, 3, 4].

The main merits of TOF cameras are high area resolution, high measurement speed, and no image processing needs. For instance the SwissRanger™ SR-3000 (http://www.swissranger.ch/), can measure depth images with spatial resolution of 176 x 144 pixels at full video rate (25 images per second). This camera uses the phase shift of modulated light to determine the range. Kahlmann et al.[2] measured the precision to be in the range of a centimetre for good conditions, with a measuring range up to 7.5 meters.

*trk@sintef.no; phone +47 22 06 73 00; fax: +47 22 06 73 50; www.sintef.no/omd.

However, cameras based on phase shift measurements are susceptible to several error sources, of which some are intrinsic in the optical system as well as the scene itself [5], and hence can not be fully eliminated by improved hardware design. These effects can cause systematic errors that are significantly greater than the measurement precision, and thus need to be calibrated or compensated for. Kahlmann et al [2, 6] discuss some of these error sources.

In this article we investigate the possibilities of modelling and compensating for measurement errors caused by light scattering in the imaging system due to poor quality of the lens system and multiple reflections within the optical lens and the camera house. The scattering effect is non-local and light from a single point in the image will affect a large region of the image, and will be added to the focused light received at each pixel. Since the scattered light generally originates from objects in the scene that are at different distances this light will have different phase shifts. When added to the focused light this will cause a phase shift that gives an error in the measured distance. With the SwissRanger™ SR-3000 we have experienced situations where the range error in the darker regions of the image can be meters, whereas the precision (repetition accuracy) may be in the range of centimetres (Figure 1).

Mure-Dubois et al.[6, 8] perform de-convolution of the scattering effect by applying a filter that approximates the inverse of the PSF. Inversion of a general PSF is difficult. They thus limit themselves to a PSF that is a sum of three Gaussian spread functions, and the PSF is assumed constant over the image area. It is found here that both of these constraints are far from realistic. This will be further discussed in section 4 (Figure 6).

In this paper it is demonstrated how we can obtain an empirical model for the Point Spread Function (PSF) of the camera that varies over the image range, and how this model can be applied in an iterative algorithm for the prediction and compensation of the range distortions. Iterative methods have long been popular for image restoration for many reasons. Firstly, they do not require computation of the inverse PDF model and secondly they allow for spatially variant PDFs. They are robust to small errors on the PDF and regularization terms and priors can easily be included to reduce noise and errors. For a tutorial on iterative image restoration methods see e.g. Katsaggelos [9].

By doing the compensation sequentially from the brightest to the darker regions of the image it is demonstrated that only one or two iterations are needed to compensate for most of the errors. With only one iteration it is typically possible to reduce the range errors by 80% of the uncompensated errors for high contrast images.

In section 2 we give a short introduction to the measurement principle of the SwissRanger™ SR-3000, and in section 3 we describe how the scattered light influences the measured range. In section 4 the proposed method and algorithm is described and test results on simulated and real data are presented in section 5. Finally a conclusion is given in section 6.

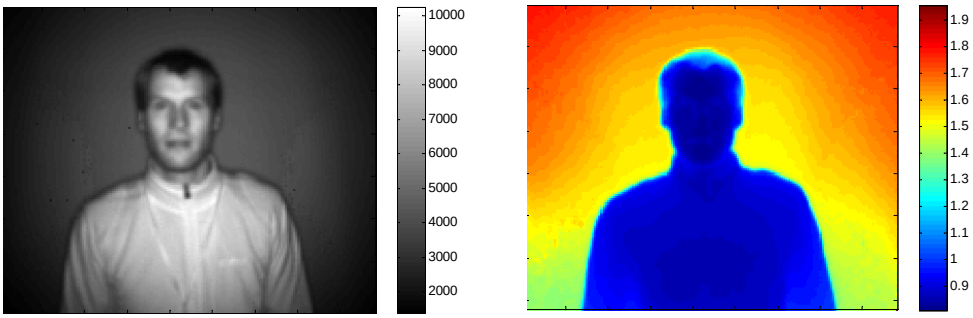

Figure 1. Image showing the distortion of the measured range in the background caused by a bright object in the foreground. On the left is the intensity image and in the right is the distance image. The true distance to the background wall is approximately 1.8 meters, whereas we see that the measured distance is as low as to 1.4 meters near the person.

2. THE MEASUREMENT PRINCIPLE

The SwissRanger™ measures the distance to the scene in each pixel by measuring the phase shift between the modulated light emitted from an array of LED's mounted on the camera face and the light reflected from the scene detected by the pixels [2,3]. At a modulation frequency f, the modulation wavelength is $\lambda = c / f$ where c is the speed of light. If the distance to the scene in a pixel is d, then the phase shift measured in that pixel is $\varphi = 2\pi(2d/\lambda)$. The modulation frequency of the SwissRanger™ can be programmed between 5 and 30 MHz, corresponding to a maximum measurement range of 30 and 5 meters respectively before wrap around occurs.

The phase of the light received at a pixel is determined by sampling the light intensity at four equally spaced times along the modulation period as illustrated in Figure 2 [2]. The measurement at each of the four sample points is an integration over many modulation periods, where the signal is integrated over a short time interval Δt in each period. The total integration time can be programmed.

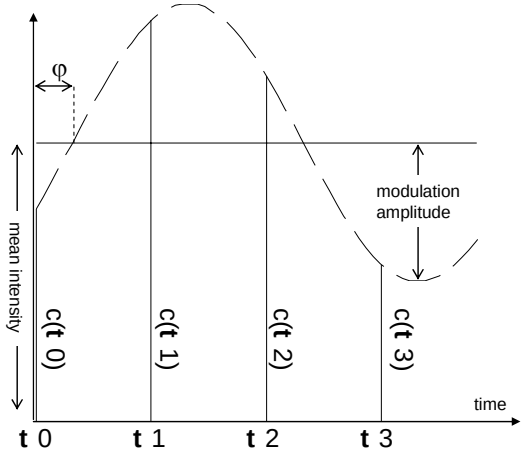

Figure 2. Illustration of the light intensity sampling at four points during the modulation period.

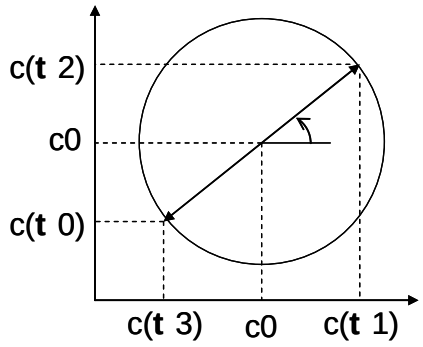

Figure 3. Illustration of the four sampled measurements at four orthogonal phase angles. The centre c0 represents the mean intensity (ambient light added modulated light).

Figure 3 illustrates the four measurements as projections on to orthogonal axes where c(τ0) and c(τ2) represents , for example, measurements at 0 and π phase shifts, and c(τ1) and c(τ3) represents measurements at π/2 and 3π/2 phase shifts. From this the phase shift φ can be computed as $\varphi = \text{atan}(\frac{c(\tau 2) - c(\tau 0)}{c(\tau 1) - c(\tau 3)})$ and the modulation amplitude A as $A = \frac{\sqrt{(c(\tau 1) - c(\tau 3))^2 + (c(\tau 2) - c(\tau 0))^2}}{2}$. These two values are returned from the SwissRanger™ SR-3000 camera for each pixel.

3. THE EFFECT OF LIGHT SCATTERING IN THE LENS AND CAMERA

In terms of scattering no camera or lens is perfect. The light returned from the scene will always be scattered to some extent over the image due to multiple reflection within the optical lens and camera housing and poor quality lenses. In typical imaging this can be insignificant, but with very bright spots in the image, such as the sun, these effects can often become more noticable.

For range imaging cameras, however, such effects can have severe implications on the measurement accuracy [9]. Since the modulated light is radiated spherically from the source located at the camera the illumination decays with the

distance r as $I = I_0 / r^2$, where I_0 is the intensity at unit distance. If, for instance, there is an object at 0.5 meters from the camera and another at 5 meters, the close up object will be illuminated with 100 times the intensity of the distant object. Hence, if one percent of the light from the bright object is scattered to the darker parts of the image, the scattered light will in practice have a similar modulation amplitude as the light received from the darker object.

Figure 4 illustrates two cases illustrating how such scattered light effects the measured distance. In both cases we have used 20 MHz modulation frequency, which gives 48 degrees phase shift per meter distance. Figure 4 a) illustrates the case discussed above, with a bright object at 0.5 meters and a darker object at 5 meters. In this case the intensity of the scattered light from the foreground object, I_s, is somewhat larger than the focused light from the background object, I_f. The phase shifts for I_f and I_s will be $\varphi_f = 240$ degrees and $\varphi_s = 240$ degrees, respectively. The resulting measured phase φ_m will be around 10 degrees, i.e. the distant object will be measured to be closer to the camera than the nearby object.

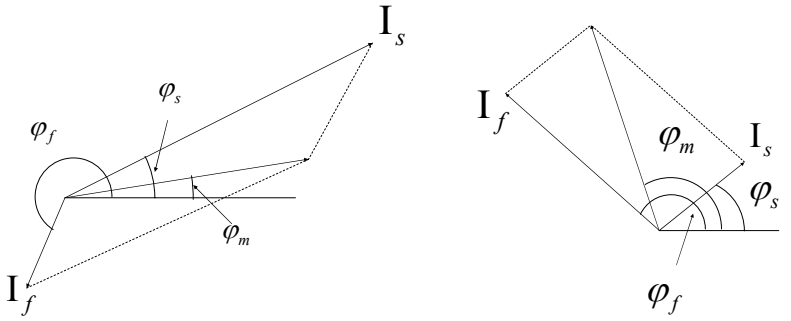

(a) (b)

Figure 4. Illustration of the effect of scattered light on the phase and distance measurement. The vectors I_f and I_s represent the focused and the scattered light. Similarly φ_f, φ_s *and* φ_m represent the phase of the focused, scattered and measured light.

Figure 4 b) illustrates a case where the object is 3 meters away and the amplitude of the light focused from that object is about twice the amplitude of the light scattered from the object close by. In this case the distant object is measured to be at approximately 2 meters instead of the true distance; 3 meters.

As seen from these two cases the effect of scattered light depends on both the relative amplitudes of the scattered versus the focused light, as well as the difference in phase angles for the two and predicting this effect is not intuitive.

4. PROPOSED METHOD FOR COMPENSATING THE EFFECT OF SCATTERED LIGHT

Mure-Dubois et al. [6] use a model for the PSF that is a sum of Gaussian functions that are constant over the image area. With this assumption they are able to design an inverse filter for de-convolving the effect of scattering. As can be seen in Figure 6, this is a very coarse approximation when compared to the experimentally obtained PSFs. The approach described here is to establish a set of empirical non-parametric scatter functions, each representing the scatter from different points in the image. The inversion of such a non-parametric and space varying PSF is difficult and an attempt to do a de-convolution as in Mure-Dubois et al. [6] is thus inappropriate. Instead an algorithm is proposed, where the model is used in a forward mode, to estimate the scattering, starting with removing the effects from the brightest parts of the image, and then sequentially remove the effects from the least bright parts. The effect of the scatter can then be subtracted from the measured image. This procedure can be repeated iteratively if required. This method is corresponding to iterative methods commonly used in image restoration [9].

Let $I(x,y)$ be a scalar field of complex numbers defined over the image area $\{x, y\} \in \Omega$ that represents the measured modulation amplitude and phase. The light received and measured at a point *x, y* is the sum of the focused light, $I_f(x,y)$, and the scattered light, $I_s(x,y)$, i.e.

$$I(x,y) = I_f(x,y) + I_s(x,y) \quad (1)$$

As illustrated in Figure 4, the scattered light variable, I_s, in (1) will influnce both on the amplitude and the phase in the resulting image, $I(x,y)$, causing measurement errors. Now, let $m(x,y,x_c,y_c)$ represent an empirically obtained PSF that predicts the intensity of the scattered light at image location *x, y,* from a light spot with unit intensity, located at x_c, y_c in the image. Since the focused light received on the sensor at point x_c, y_c is proportional to the scene intensity at this point, we can estimate the scatter from location x_c, y_c as

$$I_f(x_c,y_c) \cdot m(x,y,x_c,y_c) \quad (2)$$

and the total scatter over the image can be computed as

$$I_s(x,y) = \int_{x_c,y_c \in \Omega} I_f(x_c,y_c) \cdot m(x,y,x_c,y_c) \quad (3)$$

Typically only $I(x,y)$ in (1) is measured and thus (3) can not be employed directly since $I_f(x_c,y_c)$ is unknown. It is however reasonable to assume that the intensity of the scattered light is low compared to the focused light and therefore acceptable to start the iterative restoration procedure assuming the measured image is approximately equal to the focused image, i.e. $\hat{I}_f(x,y) = I(x,y)$, and inserting this into (3) to compute an estimate for the scattered light $\hat{I}_s(x,y)$. This can then be used to compute an updated version of the focused light, $\hat{I}_f(x,y) = I(x,y) - \hat{I}_s(x,y)$, and the procedure can be repeated iteratively [9]. To improve the convergence speed and robustness of the process it can be assumed that the light scattered from the bright parts of the image has much stronger influence on dark regions than vice versa.

Assume, for instance, an image with an object at a distance of 1 meter and a background at 2 meters. If both have a similar reflectance, the intensity of the foreground will then be 4 times that of the background. Scatter from the foreground onto the background will be proportional to foreground intensity multiplied by the foreground area. In the case where the foreground and background cover similar areas, the scatter from the foreground will be 4 times stronger than that from the background, and, since the influence of the scatter is proportional to its strength relative to the focused light, the influence from the foreground on the background will be $4 \cdot 4 = 16$ times stronger than the other way.

If we start with computing the scatter from the brightest parts of the image first, then the initial estimate $\hat{I}_f(x,y) = I(x,y)$ will be quite accurate for these regions. By subtracting the effect from this scatter from the remaining of the image before computing the scatter from the next brightest parts, the initial estimate for the second brightest parts will also be quite accurate, and so on. Our experiments indicate that only one, or at the most two iterations are needed to get good results.

The algorithm is described in Figure 5. The scatter estimation and compensation is done iteratively over $k = \{1,2,3,...,N\}$ iterations. For iteration *k* the scatter is computed in M_k steps, $i = \{1,2,3,...,M_k\}$, starting with computing and compensating the scatter from the brightest regions of the image and sequentially moving to the less bright regions until the scatter from the whole image is compensated. The region from which the scatter is computed in step *i* is defined as the parts of the image with intensity levels between the thresholds θ_{i-1} and θ_i. In the reported results $N = 2$, $M_1 = 4$ in the first iteration and $M_2 = 1$ in the second iteration.

The integral in Figure 5 is computed by convolving the PSF with the image. The space dependency of the PSF is implemented by switching between different PSFs as the convolution progresses over the image. For each step *i* in the

algorithm the convolution is calculated over the selected regions in Ω_i. After one iteration of k, the total computation corresponds to one convolution of the whole complex image with a real filter of equal size as the image. This takes 2.5 seconds on a Pentium 4, 3.2 GHz for a 25.000 pixel image as produced by the SwissRanger™ SR-3000. A significant decrease in computational speed could be obtained by approximating the 2D PSF-filters as a composition of several 1D filters. However, this possibility has not been exploited here.

1. Initialize with

$$\hat{I}_f(x,y) \leftarrow I(x,y)$$
$$\hat{I}_s(x,y) \leftarrow 0$$
$$\theta_0 \leftarrow \sup_{\{x,y\} \in \Omega} \left(\left\| I(x,y) \right\| \right)$$

2. for $k = \{1,2,3,...,N\}$ do
   for $i = \{1,2,3,...,M_k\}$ do

$$\theta_i \leftarrow \frac{M_k - i}{M_k} \cdot \theta_0$$
$$\Omega_i \leftarrow \{x,y \mid \theta_{i-1} \geq \left\| I(x,y) \right\| > \theta_i\}$$
$$\hat{I}_s(x,y) \leftarrow \hat{I}_s(x,y) + \int_{x_c,y_c \in \Omega_i} \hat{I}_f(x_c,y_c) \cdot m(x,y,x_c,y_c)$$
$$\hat{I}_f(x,y) \leftarrow I(x,y) - \hat{I}_s(x,y)$$

Figure 5. Iterative sequential algorithm for the removal of scattered light from the measured amplitude and phase image.

5. EMPIRICAL DETERMINATION OF SCATTER MODELS

An empirical scatter model was obtained for the SwissRanger™ SR-3000 camera by placing a small circular (19 mm diameter) retro-reflective reflector, with a flat top onto a planar black sheet. In order to avoid saturation of the camera sensor the integration time of the camera was reduced to 512 μs, resulting in a modulation amplitude received at the reflector of 15 000-20 000 units, whereas the intensity measured on the black sheet without the reflector was between 10 units in the corners and 400 units in the middle. (The modulation amplitudes presented here are in arbitrary units as returned by the camera). Since both the reflector and the dark sheet are at the same distance from the camera (approximately 1.2 m), all received light will have a similar phase and we need not consider phase when we add and subtract intensities. Each scatter and background measurement is an average of 10 subsequent images.

Figure 6 shows some examples of measured light scatter for different placements of the reflector. The reflector itself covers approximately 3 x 3 pixels in the image. The amplitude images shown in Figure 6 are obtained by subtracting the amplitudes measured with the background without the reflector, and therefore represent the scattered light only. The amplitude of the side lobes seen in upper left image is around 20 units, which is approximately 0.1 % of the reflector amplitude.

It is clear that the scatter pattern is far from Gaussian and varies significantly from according to placement in the image. We therefore decided to develop independent empirical non-symmetric models for the reflector placed in 7 x 5 different positions making a grid pattern over the image area. When later applying these models for predicting the total scatter, the model that was based on the reflector position nearest to the actual pixel in the image was used. To allow inclusion of the areas at the borders of the image the scatter models needed to be extrapolated around 10 pixels outside the measured range. This was done based on simple symmetry considerations.

The scatter models were normalized in amplitude to represent the scatter of a light spot in the scene with an area corresponding to one pixel, and with modulation amplitude one. This was done by dividing the measured image with the integral of the intensity amplitudes within the area of the reflector (approximately 3 x 3 pixels). Finally, the pixels within the area of the reflector were set to the level of the surrounding pixels, thus modelling the scattered light only.

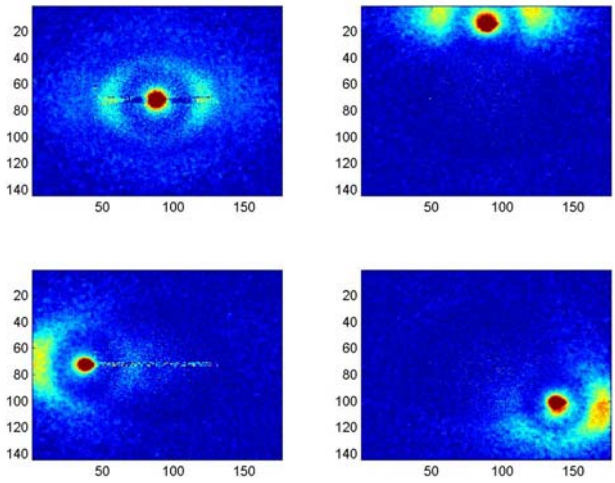

Figure 6. Distribution of the scattered light for different placements of the reflector in the image.

6. EXPERIMENTAL RESULTS

Figure 7 shows the simulated case used to evaluate the potential of the algorithm in removing the effects of scatter. Three boxes are placed at 0.5, 1 and 2 meters distance from the camera. The background is at 5 meters. All objects and the background are assumed to have the same reflectivity, giving them relative intensities 100, 25, 6 and 1 respectively. The empirically obtained scatter models as illustrated in Figure 6 were then applied to the idealized synthetic image to get the synthetic image shown in Figure 7 upper left and upper right. In this case it is seen that the scatter from the foreground image causes the background to be measured closer to the camera than the foremost object. This corresponds to the situation in Figure 4 a). The algorithm was then applied to this synthetic image using the same PDFs. Figure 7 shows, in the lower left graph, a horizontal intersection across all three objects. The red and green traces show the measured distance after one and two iterations of the compensation algorithm. The true distance is plotted in black, which is not clearly visible behind the green. The lower right graph shows a vertical cross section across the middle and front objects. It is clear, almost all the error is removed in one iteration and after two iterations no detectable error remains.

A real scene similar to the synthetic scene is shown in Figure 8. Cardboard boxes used as objects are placed at 0.5, 1, and 2 meters distances; the background is at 5 meters. The intensities measured for these objects were 8611, 3774, 954, 213 in average, respectively. There was natural ambient light in the room. We here demonstrate in real life the effect of the scattering causing the background to appear closer than the foremost object. Most of this error was removed by one iteration of our algorithm. However a compensation overshoot can be observed in the background adjacent to the objects. The cause for this error has not been investigated. This error increases after the second iteration, and thus the average error over the whole scene increases.

Figure 9 shows the result obtained for the image shown in Figure 1. The measurements with and without compensation are shown for three horizontal lines across the image. Again the algorithm is seen to compensate for the errors quite well, except for the lowest horizontal intersection where the errors are largest.

Table 1 summarizes the achieved accuracy over the image areas.

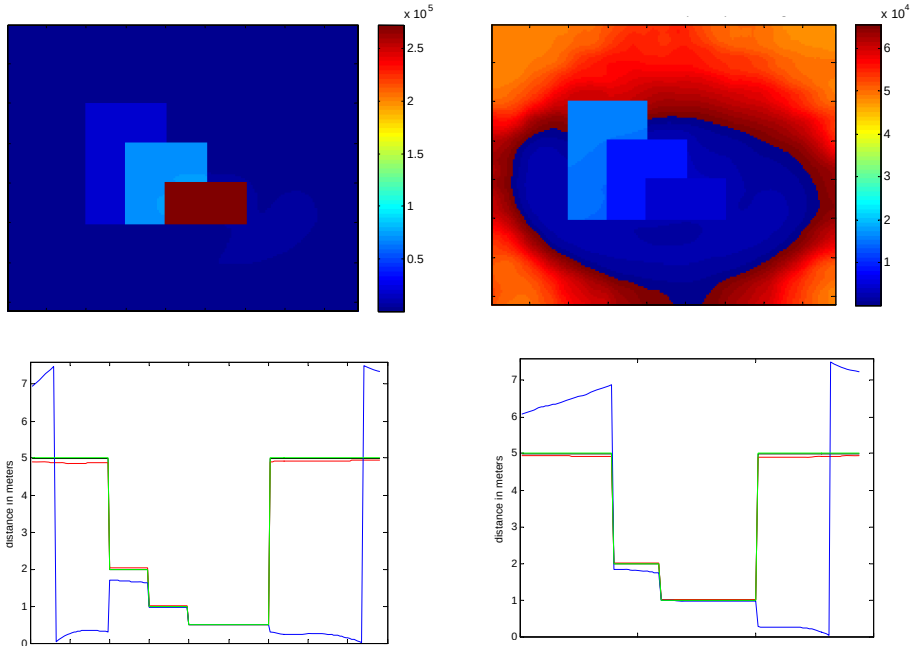

Figure 7: Synthetic intensity (upper left) and phase (upper right) image. The lower left shows a horizontal intersection across the three objects, and the lower right shows a vertical intersection across the middle and front object. Blue: Measured distance. Red: Result after one iteration of compensation algorithm. Green: Result after two iterations. Black: True distance, partly not visible behind the green.

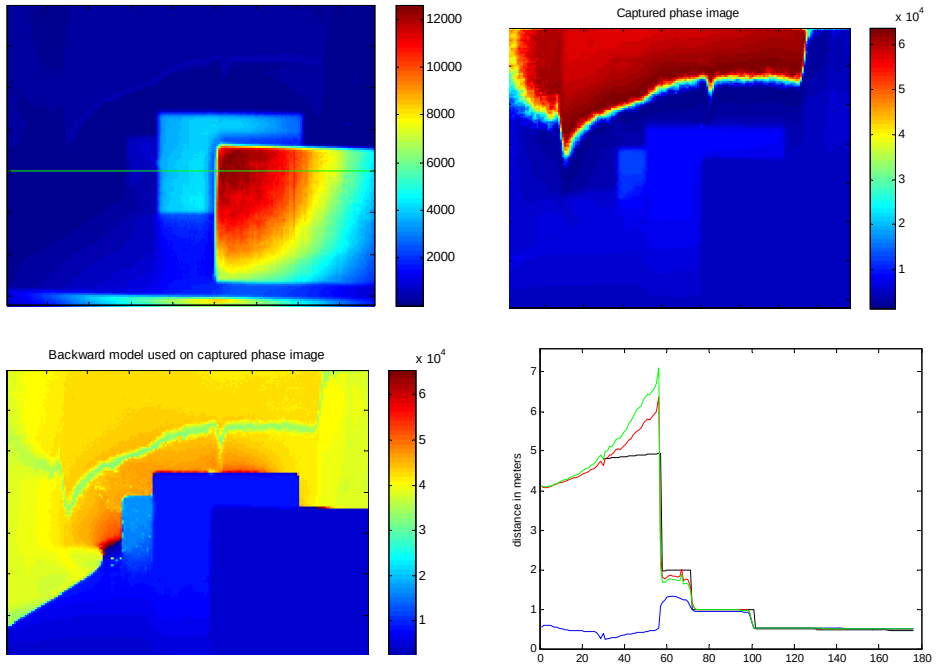

Figure 8. Image of real scene similar to the theoretical scene in Figure 7. Intensity (upper left), captured phase (upper right), and corrected phase (lower left) images are shown. Due to the side walls in the room the measuring area is between columns 30 and 150. The graph (lower right) shows the measured distances along the horizontal line in the upper left image. Blue: Measured distance. Red: Result after one iteration of compensation algorithm. Green: Result after two iterations. Black: Theoretical measured background distance.

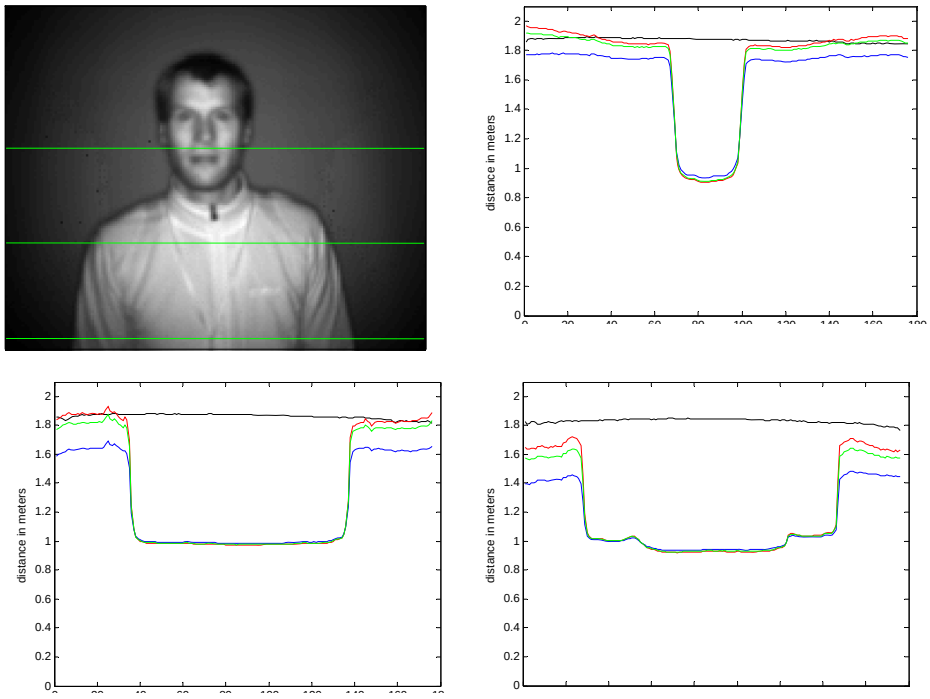

Figure 9. Graphs show the measured distances along the three horizontal lines in the upper left image. Upper right is across face, lower left is across shoulders and lower right is across chest. Blue: Measured distance. Red: Result after one iteration of compensation algorithm. Green: Result after two iterations. Black: Measured background distance.

Table 1. Average of absolute measurement errors before and after applying the compensation algorithm. For the synthetic image and for the real scene simulating the synthetic scene results are shown for the whole image and for the background only. For the image with a person the figures correspond to the background only since the true distance is unknown for the foreground. In parenthesis is the fraction of the error compensated.

Image	**0 iteration**	**1 iteration**	**2 iterations**
Synthetic (whole image)	2.25m	0.0633m (97.2%)	0. 0065m (99.7%)
Synthetic (background)	2.62m	0.0724m (97.2%)	0.0074m (99.7%)
Real scene (whole image)	1.41m	0.1660m (88.2%)	0.2115m (85.0%)
Real scene (background)	2.97m	0.2956m (90,1%)	0.3940m (86.8%)
Person (background)	0.1543m	0.1063m (31.1%)	0.0537m (65.2%)

7. CONCLUSION

Range imaging cameras that measure the time of flight based on phase measurements are shown to be susceptible to severe distortions in the measured range caused by light scattering within the lens and camera. A method is proposed for how to establish and use empirical models for this scatter to estimate and compensate for such distortions. The otherwise difficult inverse problem is solved by using of a forward model iteratively. Each iteration is done as a sequential process, starting with the brightest parts of the image and then moving sequentially to the least bright parts, subtracting the estimated effects from the measurements at each step. An average reduction of the measurement error by at least 40% or better compared to the uncompensated measurements was demonstrated on realistic images, i.e. more than 60% of the

error is compensated for by our method. The computation load for one iteration of the algorithm corresponds to a convolution of the measured complex image with a real filter of the same size. This takes around 2.5 seconds on a 3.2 GHz Pentium 4 for a 25.000 pixel image as produced by the SwissRanger™ SR-3000.

REFERENCES

[1] C.Niclass, P.-A. Besse, E. Charbon, "Arrays of Single Photon Avalanche Diodes in CMOS Technology: Picosecond Timing Resolution for Range Imaging". Proceedings of the 1st Range Imaging Research Day at ETH Zurich, Zurich, Switzerland, pp. "Supplement to the Proceedings", 2005.

[2] T. Kahlmann, F. Remondino, H. Ingensand, "Calibration for increased accuracy of the range imaging camera SwissRanger™", IAPRS Volume XXXVI, Part 5, Dresden, 25-27 September 2006.

[3] T. Kahlmann and H. Ingensand, "Calibration of the fast range imaging camera SwissRanger™ for use in the surveillance of the environment". Electro-Optical Remote Sensing II, Edited by G.W. Kamerman, D.V. Willetts, E. K. Steinvall, Proc. of SPIE Vol. 6396, 639605. 2006

[4] S. Gokturk, H. Yalcin, and C. Bamji. "A Time-Of-Flight Depth Sensor - System Description, Issues and Solutions.", Proceedings of IEEE Conf. CVPR, Washington D.C., USA, June 2004.

[5] D, Falie, V, Buzuloiu, "Noise characteristics of 3D time-of-flight cameras", ISSCS, 2007.

[6] T. Kahlmann and H. Ingensand, "Calibration and improvements of the high-resolution range-imaging camera SwissRanger". Videometrics VIII, J.-Angelo Beraldin, Sabry F. El-Hakim, Armin Gruen, James S. Walton, Editors, January 2005, pp. 144-155 Proceedings of SPIE -- Volume 5665, 2005.

[7] J. Mure-Dubois and H. Hügli, "Optimized scattering compensation for time of flight camera", Two- and Three-Dimensional Methods for Inspection and Metrology V, edited by Peisen S. Huang, Proceedings of SPIE Vol. 6762, 67620H, 2007a.

[8] J. Mure-Dubois and H. Hügli, "Real-time scattering compensation for time-of-flight camera", Proceedings Of the ICVS 2007, Feb. 2007b.

[9] T. Kahlmann and H. Ingensand, "Increased accuracy of 3D range image camera by means of calibration", 8th Conference on Optical 3-D Measurement Techniques, Zurich, 9-12 July, 2007.

[10] A. K. Katsaggelos, "Iterative image restoration algorithms", Optical Engineering, pp. 735 – 748, Vol. 28 No.7, 1989.